A Half-Moon Antenna

NAKANO, Hisamatsu / YAMAUCHI, Junji / HITOSUGI, Kazuo / SETO, Masaaki / YAMAMOTO, Yusuke

(出版者 / Publisher)
IEEE

(雑誌名 / Journal or Publication Title)
IEEE Transactions on Antennas and Propagation / IEEE Transactions on Antennas and Propagation

(号 / Number)
12

(開始ページ / Start Page)
3237

(終了ページ / End Page)
3244

(発行年 / Year)
2004-12

A Half-Moon Antenna

Hisamatsu Nakano, *Fellow, IEEE*, Yusuke Yamamoto, Masaaki Seto, Kazuo Hitosugi, and Junji Yamauchi, *Member, IEEE*

***Abstract*—This paper presents a half-moon antenna (HMA), which is composed of two semi-circular top and bottom conducting plates joined by a rectangular conducting plate. The HMA has a wide radiation beam. Radiation in the $y-z$ plane (in the E plane) is hemispherical with a half-power beam width (HPBW) of more than 200°. Radiation in the $x-y$ plane (in the H plane) forms a sector beam with an HPBW of more than 100°. To reduce the backward radiation and improve the gain, chokes are added to the HMA. An increase in the gain of approximately 1 dB is obtained. In order to obtain a tilted beam, the radius of the bottom plate is reduced. The maximum beam direction of the tilted beam $\theta_{\max}$ is not sensitive to frequency. Within a frequency range of 11 to 14 GHz (24%), $\theta_{\max} = 167° \pm 2°$. The gain is found to be $G = 9.5 \pm 0.5$ dBi within this same frequency range.**

***Index Terms*—Cylindrical finite-difference time-domain (FDTD) method, small aperture antenna, tilted beam formation, wide radiation.**

I. Introduction

J. J. EPIS HAS investigated a radial-mode horn, which consists of a wave-launching section and a radial section [1]. The wave-launching section is made of a rectangular waveguide and the launched cylindrical wave radiates from the cylindrical aperture of the radial section. It has been revealed that the radial-mode horn can provide a relatively flat-topped radiation pattern in the H plane.

The increasing popularity of wireless LAN systems has created the need for an antenna with a wide radiation beam and a simple structure. This paper presents a half-moon antenna (HMA), which has a simple structure and a wide radiation beam suitable for such an application. The HMA is composed of two parallel semi-circular conducting plates and a rectangular conducting plate joining the two parallel plates, as shown in Fig. 1. A probe near the rectangular plate (rear wall) feeds the antenna. It can be said that the HMA has a simpler structure than the radial-mode horn.

The purpose of this paper is to reveal the antenna characteristics of the HMA. We use the finite-difference time-domain (FDTD) method [2]–[5] as the analysis method to achieve this purpose. First, therefore, we briefly summarize the FDTD method, which is formulated using a cylindrical coordinate system.

Manuscript received November 12, 2002; revised March 6, 2004.

H. Nakano, K. Hitosugi, and J. Yamauchi are with the College of Engineering, Hosei University, Tokyo 184-8584, Japan (e-mail: nakano@k.hosei.ac.jp).

Y. Yamamoto was with the College of Engineering, Hosei University, Koganei, Tokyo 184-8584, Japan. He is now with Canon NTC, Incorporated, Tokyo 104-0031, Japan.

M. Seto was with the College of Engineering, Hosei University, Tokyo 184-8584, Japan. He is now with NEC Corporation, Tokyo 108-8001, Japan.

Digital Object Identifier 10.1109/TAP.2004.836427

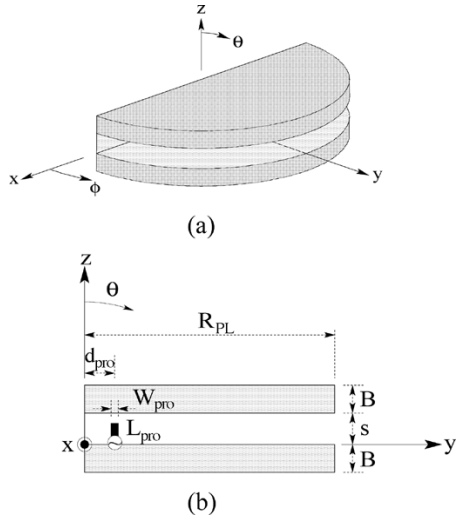

Fig. 1. Configuration of an HMA. (a) Perspective view and (b) side view.

Second, the analysis results are presented and discussed. Effects of the size and thickness of the semi-circular parallel conducting plates on the radiation pattern are revealed and a technique for reducing the backward radiation is presented. It is shown that adding chokes to the parallel plates contributes to a reduction in the backward radiation. Third, the frequency responses of the input impedance and gain of the HMA with chokes are evaluated and discussed.

Finally, we investigate tilted beam formation, without the use of conventional array techniques, using a modified HMA, where the top and bottom plates have different radii, as shown in Fig. 10. A tilted beam is useful in LAN base station antenna applications. The beam direction as a function of the radius of the bottom plate is evaluated. Furthermore, the beam direction as a function of frequency is calculated and the frequency response of the gain is also revealed.

Note that the analysis is performed using a frequency band of 11 to 14 GHz (24%) and some experimental results are presented to confirm the analysis.

II. Configuration

Fig. 1 shows the configuration of an HMA [6]–[8]. The antenna is composed of two semi-circular conducting plates parallel to each other. The linear edges of these two plates are joined by a rectangular conducting plate (referred to as the rear wall). A strip probe connected to the inner conductor of a coaxial line close to the rear wall feeds the antenna.

The notation is as follows: $R_{\rm PL}$ is the radius of the semi-circular conducting plate; B is the thickness of the semi-circular conducting plate; s is the spacing between the two semi-circular

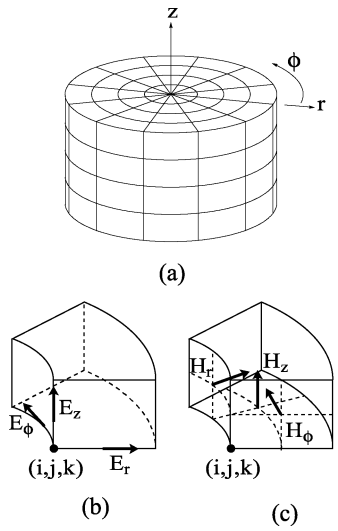

Fig. 2. FDTD method based on a cylindrical coordinate system.

conducting plates; $W_{\rm pro}$ and $L_{\rm pro}$ are the width and length of the feed strip probe, respectively; and $d_{\rm pro}$ is the distance from the rear wall to the center of the feed probe.

III. Summary of Analysis Techniques

We analyze the HMA using an FDTD method. Use of the Yee mesh based on rectangular coordinates (x, y, z) [3] causes error due to a staircase approximation of the curved edges of the top and bottom plates. To avoid this error, we adopt cylindrical coordinates $(r, \phi, z) = (i\Delta r, j\Delta\phi, k\Delta z)$ with a time coordinate $t = n\Delta t$ and formulate Maxwell's curl equations for electric field $\mathbf{E}(t)$ and magnetic field $\mathbf{H}(t)$.

Field components $E_r(i + (1/2), j, k)$, $E_\phi(i, j + (1/2), k)$, $E_z(i, j, k + (1/2))$, $H_r(i, j + (1/2), k + (1/2))$, $H_\phi(i + (1/2), j, k + (1/2))$, and $H_z(i + (1/2), j + (1/2), k)$ are assigned as shown in Fig. 2. The finite difference expression for the field component [15], for example, E_r, is obtained from

$$\varepsilon \frac{\partial E_r}{\partial t} = \frac{1}{r}\frac{\partial H_z}{\partial \phi} - \frac{\partial H_\phi}{\partial z} \tag{1}$$

as

$$\begin{aligned} E_r^n &\left(i+\frac{1}{2}, j, k\right) \\ &= E_r^{n-1}\left(i+\frac{1}{2}, j, k\right) + \frac{\Delta t}{\varepsilon r_{i+\frac{1}{2}}\Delta\phi} \\ &\quad \times \left[H_z^{n-\frac{1}{2}}\left(i+\frac{1}{2}, j+\frac{1}{2}, k\right)\right. \\ &\qquad \left. - H_z^{n-\frac{1}{2}}\left(i+\frac{1}{2}, j-\frac{1}{2}, k\right)\right] \\ &\quad - \frac{\Delta t}{\varepsilon \Delta z}\left[H_\phi^{n-\frac{1}{2}}\left(i+\frac{1}{2}, j, k+\frac{1}{2}\right)\right. \\ &\qquad \left. - H_\phi^{n-\frac{1}{2}}\left(i+\frac{1}{2}, j, k-\frac{1}{2}\right)\right]. \end{aligned} \tag{2}$$

It should be noted that 1) E_ϕ and H_r at $r = 0$ (i.e., $i = 0$) are not needed to update the field components, and 2) E_z has a singularity when $r = 0$, but the singularity can be removed

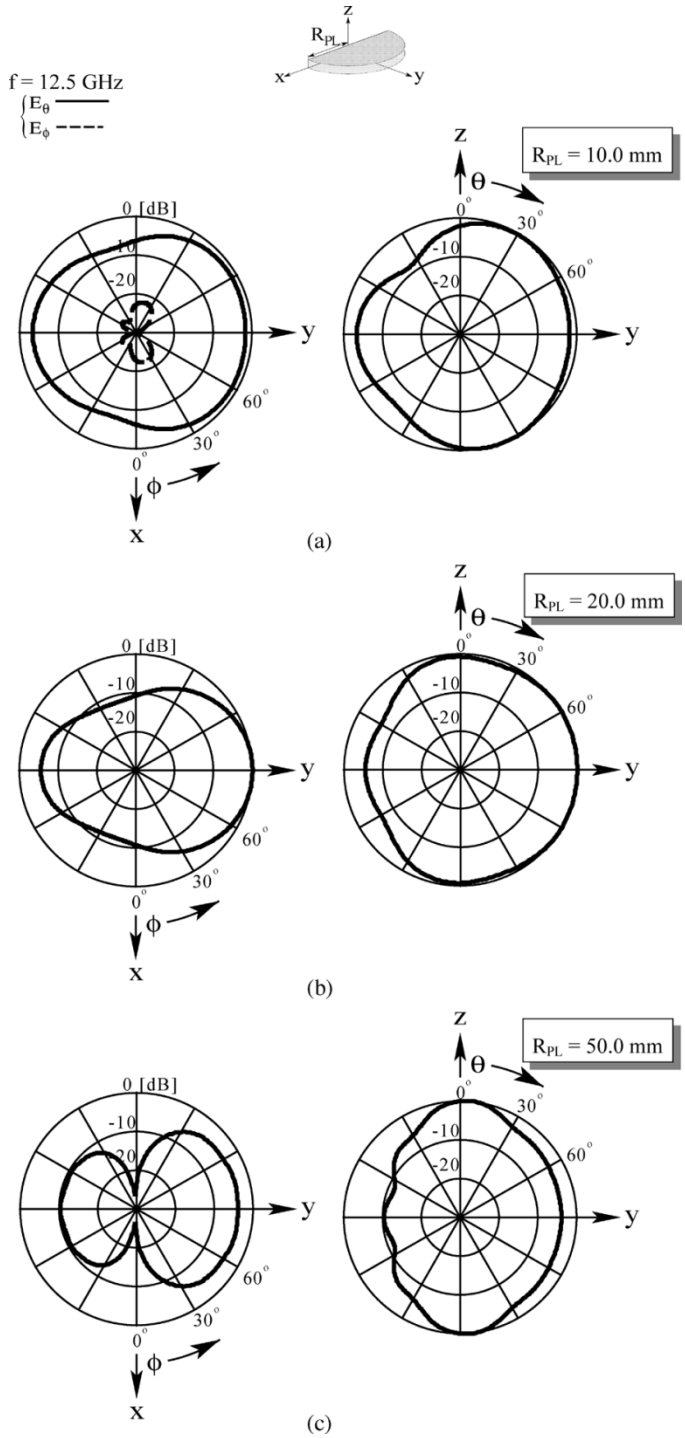

Fig. 3. Radiation patterns as a function of the radius $R_{\rm PL}$. The semi-circular plates are infinitesimally thin $(B = 0)$.

using the integral form for the curl equation $\nabla \times \mathbf{H} = \partial\mathbf{D}/\partial t$, where $\partial\mathbf{D}/\partial t$ is the displacement current density [4], [5].

An absorbing boundary condition (ABC) based on Newton's backward-difference polynomial is used to truncate the computation space. This ABC is applied to the boundaries in the r and z directions. We express the tangential electric field components E_ϕ and E_z at the boundary $r = \xi_r$ as $E_\phi(t + \Delta t, \xi_r)$ and $E_z(t + \Delta t, \xi_r)$, respectively, and denote them as $E(t + \Delta t, \xi)$ for simplicity. Similarly, we denote the tangential electric field components E_r and E_ϕ at the boundary $z = \xi_z$ as $E(t+\Delta t, \xi)$.

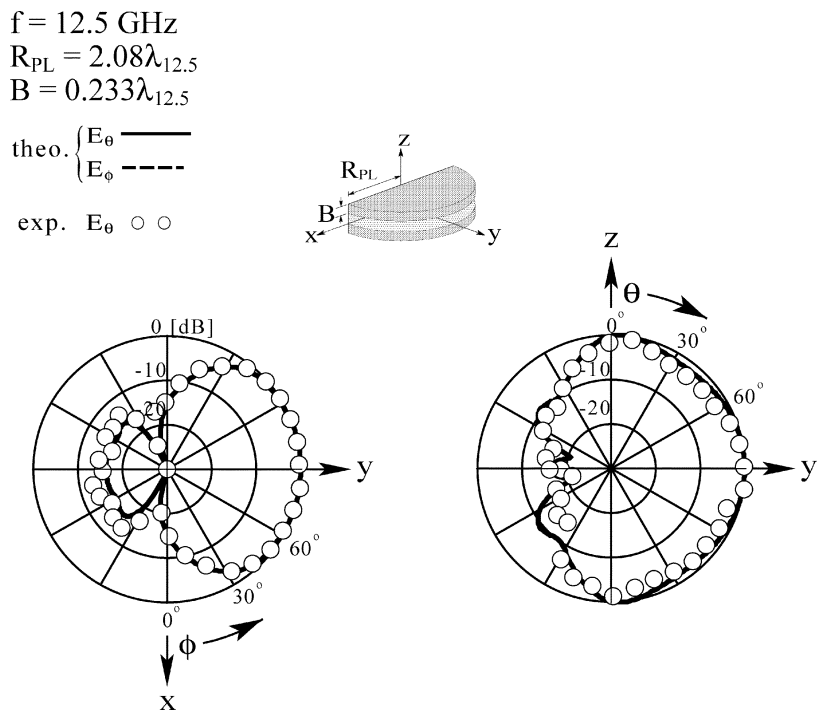

Fig. 4. Representative radiation patterns for finite thickness B. The cross-polarization component E_ϕ is less than -30 dB and does not appear in this figure.

Note that $E(t+\Delta t,\xi)$ is decomposed into $2E_1 - E_2$, where $E_1 = E(t,\xi-\alpha \mathrm{c}\Delta t)$ and $E_2(t-\Delta t,\xi-2\alpha \mathrm{c}\Delta t)$ with c and $\alpha(0\le\alpha\le 1)$ being the speed of light and a scaling factor, respectively. Extrapolation using coordinates $\xi - \mathrm{m}\Delta\xi$ ($\mathrm{m}=0$, 1, 2, 3, 4) leads to [2], [9]

$$\begin{aligned} E(t+\Delta t,\xi) = {} & 2e_1E(t,\xi)+2e_2E(t,\xi-\Delta\xi) \\ & +2e_3E(t,\xi-2\Delta\xi)-(e_1)^2E(t-\Delta t,\xi) \\ & -2e_1e_2E(t-\Delta t,\xi-\Delta\xi) \\ & -\left\{2e_1e_3+(e_2)^2\right\}E(t-\Delta t,\xi-2\Delta\xi) \\ & -2e_2e_3E(t-\Delta t,\xi-3\Delta\xi) \\ & -(e_3)^2E(t-\Delta t,\xi-4\Delta\xi) \end{aligned} \tag{3}$$

where $e_1=(2-\tau)(1-\tau)/2$, $e_2=\tau(2-\tau)$, $e_3=\tau(\tau-1)/2$ with $\tau=\alpha \mathrm{c}\Delta t/\Delta\xi$.

The radiation patterns are obtained on the basis of the equivalence theorem [10], where equivalent electric and magnetic current densities, $\mathbf{J}_s(\omega)$ and $\mathbf{M}_s(\omega)$, on an imaginary surface S enclosing the antenna are required. To meet this requirement, the time-domain electric and magnetic fields on S, $\mathbf{E}(t)$ and $\mathbf{H}(t)$, obtained using the FDTD method, are Fourier-transformed. $\mathbf{J}_s(\omega)$ and $\mathbf{M}_s(\omega)$ are given as $\mathbf{J}_s(\omega)=\hat{n}\times F[\mathbf{H}(t)]$ and $\mathbf{M}_s(\omega)=F[\mathbf{E}(t)]\times\hat{n}$, where $F[\mathbf{E}(t)]$ and $F[\mathbf{H}(t)]$ are Fourier-transforms of $\mathbf{E}(t)$ and $\mathbf{H}(t)$, respectively, and $\hat{n}$ is an outward unit vector normal to the surface S.

The input impedance $Z_{\mathrm{in}}(=R_{\mathrm{in}}+jX_{\mathrm{in}})$ is calculated as $Z_{\mathrm{in}}=F[V_{\mathrm{in}}(t)]/F[I_{\mathrm{in}}(t)]$, where $F[V_{\mathrm{in}}(t)]$ and $F[I_{\mathrm{in}}(t)]$ are Fourier-transforms of the time-domain voltage $V_{\mathrm{in}}(t)$ and current $I_{\mathrm{in}}(t)$ at the feed point, respectively. For $V_{\mathrm{in}}(t)$, we use a sine function modulated by a Gaussian function; $V_{\mathrm{in}}(t)=V_{\mathrm{gauss}}(t)\sin\omega t$, where $V_{\mathrm{gauss}}(t)=\exp\{-(t-T)/\mathrm{KT}\}^2$ with $K=0.29$ and $T=0.646/f_{3\mathrm{dB}}$. Note that $f_{3\mathrm{dB}}$ is the frequency at which the power spectrum $|F[V_{\mathrm{gauss}}(t)]|^2$ for $K=0.29$ drops 3 dB from the maximum value. The current $I_{\mathrm{in}}(t)$ is obtained by integrating the magnetic field $\mathbf{H}(t)$ around the feed probe at the input (Ampere's circuital law).

Using the Fourier-transformed value $F[I_{\mathrm{in}}(t)]$, the gain G at a far-field point of (r, θ, ϕ) is calculated to be $G = [|F[E(t)]/\sqrt{2}|^2/Z_0]/[P_{\mathrm{in}}/(4\pi r^2)]$, where $P_{\mathrm{in}}(=R_{\mathrm{in}}|F[I_{\mathrm{in}}(t)]/\sqrt{2}|^2)$ is the power input to the antenna and $Z_0(=120\pi\ \mathrm{ohms})$ is the intrinsic impedance of free-space. Note that the realized gain G_W [11], [12] is smaller than the gain G, depending on the degree of impedance mismatching between the antenna and the feed line. The G_W is given as G/M, where $M(=(1+\mathrm{VSWR})^2/(4\mathrm{VSWR})=(1-|\Gamma|^2)^{-1}$, with $|\Gamma|^2$ being the power reflection coefficient) is the reflection loss due to impedance mismatching. Using the relation $10\log G_W = 10\log G - 10\log M$, the gain 10 log G is given by adding the reflection loss 10 log M to the realized gain $10\log G_W$, that is, G in dB $=M$ in dB $+G_W$ in dB.

IV. Analysis Results

To investigate the radiation beam from the HMA in detail, we start by choosing parameters: spacing between the top and bottom plates $s=6.3\ \mathrm{mm}=0.2625\lambda_{12.5}$, strip probe width $W_{\mathrm{pro}}=1\ \mathrm{mm}=0.0417\lambda_{12.5}$, strip probe length $L_{\mathrm{pro}}=4.2\ \mathrm{mm}=0.175\lambda_{12.5}$, distance between the center of the strip probe and the rear wall $d_{\mathrm{pro}}=6\ \mathrm{mm}=\lambda_{12.5}/4$, where $\lambda_{12.5}(=24\ \mathrm{mm})$ is the wavelength at a test frequency of 12.5 GHz. To simplify the following discussion, these parameters are fixed throughout this paper. The plate thickness B and radius R_{PL} are varied subject to the objectives of the analysis. Note that the thickness of the strip probe is assumed to be infinitesimally thin.

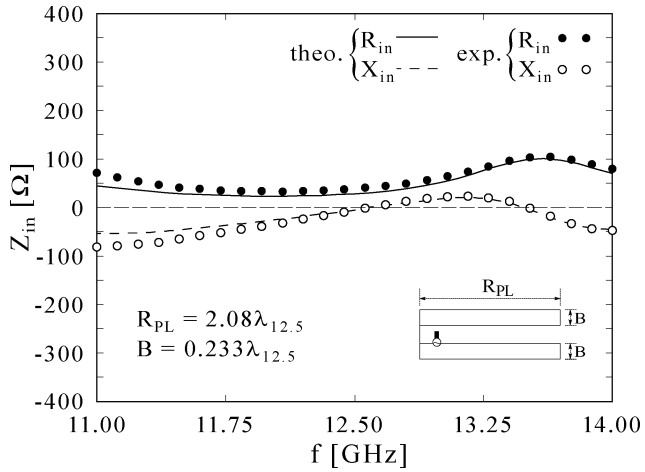

Fig. 5. Input impedance as a function of frequency.

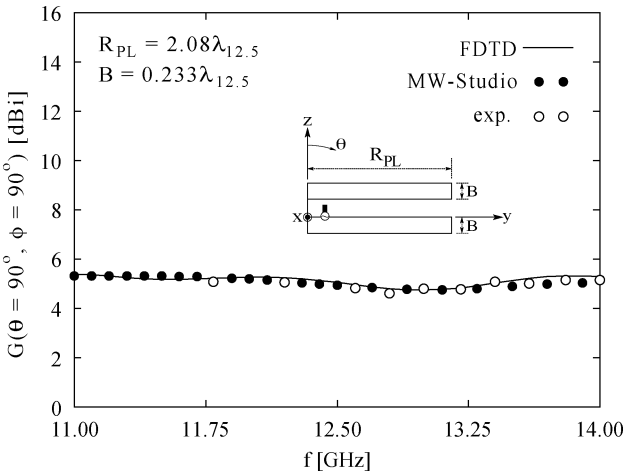

Fig. 6. Gain as a function of frequency.

A. Fundamental Antenna Characteristics

The radiation pattern at 12.5 GHz as a function of plate radius $R_{\rm PL}$ is investigated, assuming that the plate thickness is infinitesimally thin ($B = 0$). The theoretical radiation pattern at $R_{\rm PL} = 20\,{\rm mm} (= 0.833\lambda_{12.5})$ is shown in Fig. 3(b), together with patterns for $R_{\rm PL}$ less than and greater than 20 mm.

As seen from Fig. 1(b), the antenna configuration in the $y-z$ plane is not symmetric with respect to the y axis. Therefore, as the plate radius $R_{\rm PL}$ decreases (and hence the distance from the strip probe to the plate edges ($R_{\rm PL} - d_{\rm pro}$) decreases), effects of this asymmetry appear in the radiation pattern in the $y-z$ plane, as shown in Fig. 3(a), where $R_{\rm PL} - d_{\rm pro}$ is 4 mm and smaller than $d_{\rm pro} = 6\,{\rm mm}$. Conversely, the asymmetry of the radiation pattern in the $y-z$ plane almost disappears as the plate radius $R_{\rm PL}$ becomes large, as shown in Fig. 3(b) and (c).

The directivity in the y direction becomes maximal in the vicinity of $R_{\rm PL} = 20\,{\rm mm}$. The half-power beam width (HPBW) in the $x-y$ plane (in the H plane) at $R_{\rm PL} = 20\,{\rm mm}$ is calculated to be 80° [see Fig. 3(b)].

An HPBW of greater than 80° in the $x-y$ plane is obtained by increasing the plate radius $R_{\rm PL}$. A HPBW of approximately 120° is obtained at $R_{\rm PL} = 50\,{\rm mm} \equiv R_{\rm PL50} (= 2.08\lambda_{12.5})$. However, the maximum radiation in the $y-z$ plane (in the E plane) is no longer in the y direction, as shown in Fig. 3(c).

To change the maximum radiation in the $y-z$ plane from the z direction to the y direction, the thickness B is varied, while fixing the plate radius to be $R_{\rm PL50}$. It is found that, as B increases, the radiation intensity in the y-axis direction increases. Fig. 4 shows representative radiation patterns at $B = 5.6\,{\rm mm} \equiv B_{5.6} (= 0.233\lambda_{12.5})$, where the radiation intensity in the y-axis direction equals that in the z-axis direction. For confirmation of the theoretical results for $B_{5.6}$, the experimental results (white dots for the E_θ component) are also shown, where the E_ϕ component (cross-polarization component) is less than -30 dB and does not appear in this figure. Note that the radiation pattern remains almost unchanged in a range of $B = 5.6\,{\rm mm}$ to $B = 9.8\,{\rm mm}$, resulting in a nearly constant directivity in the y direction (variation of 0.1 dB).

Based on the above observation at 12.5 GHz, we choose parameters ($R_{\rm PL}$, B) to be ($R_{\rm PL50}$, $B_{5.6}$) and investigate the frequency response of the HMA. Fig. 5 shows the input impedance

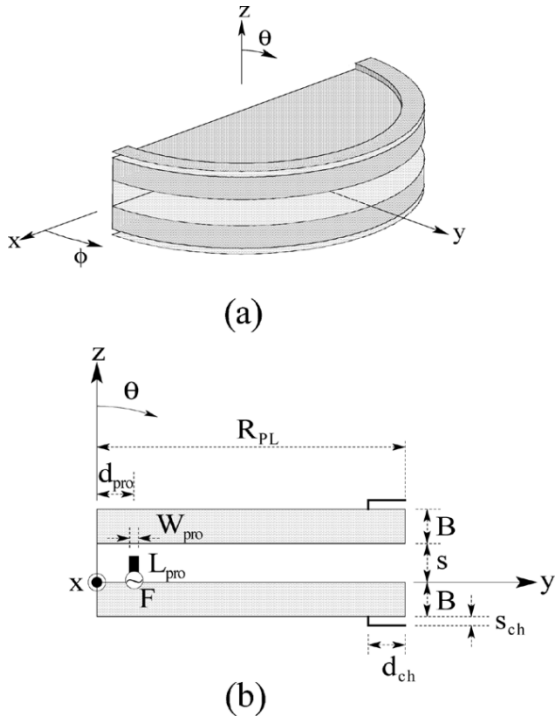

Fig. 7. Half-moon antenna with chokes. (a) Perspective view and (b) side view.

$Z_{\rm in} = R_{\rm in} + jX_{\rm in}$ as a function of frequency. A purely resistive input impedance is obtained in the vicinity of a test frequency of 12.5 GHz. The experimental results, obtained using an HP 8510C network analyzer, are close to the theoretical ones. The slight discrepancy between the theoretical and experimental results is mainly due to the difference between the theoretical and experimental feed systems: a delta-gap source is used for the theoretical feed system, while a coaxial line source is used for the experimental feed system. The theoretical delta-gap is approximated with a gap of length $\Delta = 0.015\lambda_{12.5}$ [13]. In the experiment, the radius of the inner conductor of the coaxial line feed is chosen to be the electrical equivalent radius of the theoretical strip probe ($W_{\rm pro}/4 = 0.25\,{\rm mm}$) [14]. Note that the smallest theoretical return loss is -16.4 dB at 12.9 GHz and the theoretical frequency bandwidth for a -9.54 dB return loss criterion (VSWR = 2 relative to 50 ohms) is approximately 7.9%.

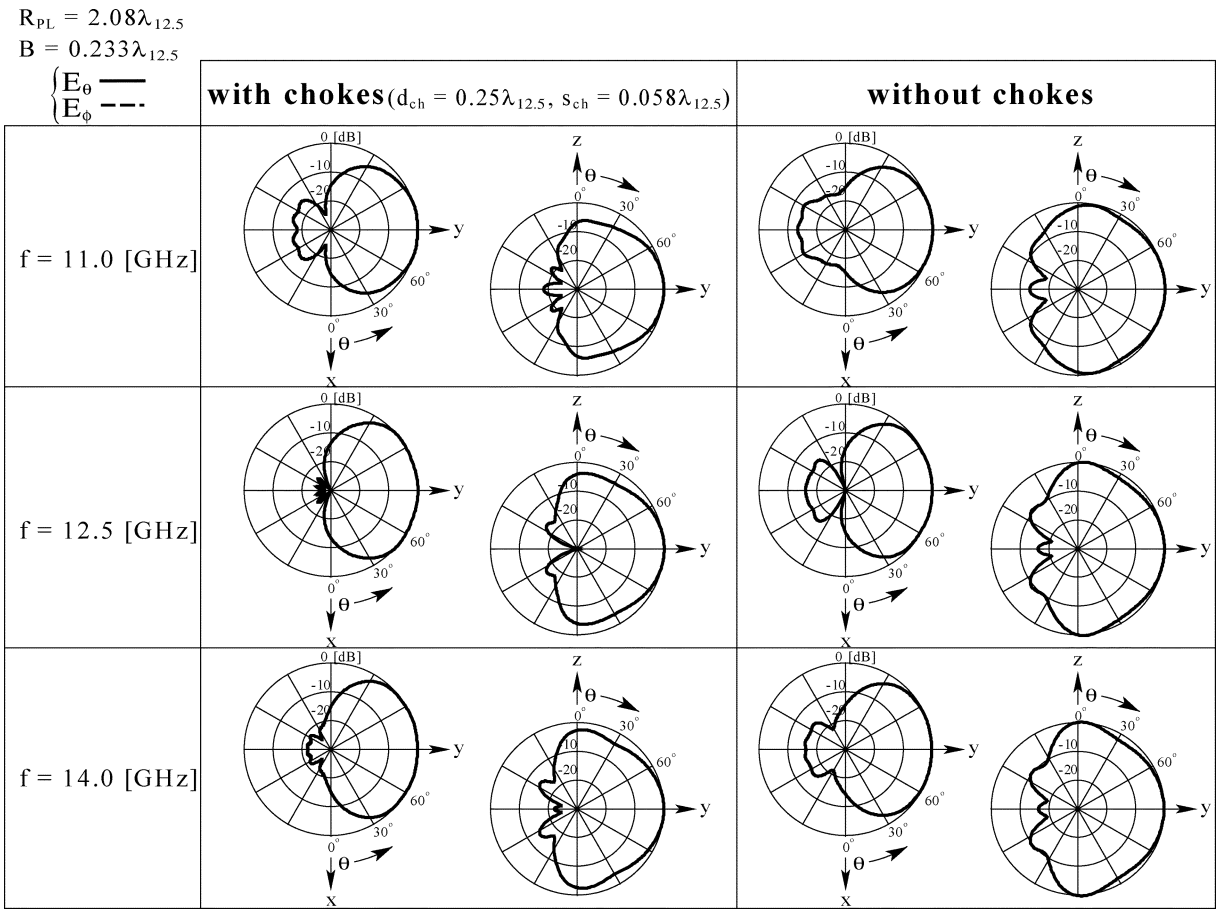

Fig. 8. Radiation patterns for half-moon antennas with and without chokes as a function of frequency.

The radiation pattern is not sensitive to frequency. The radiation in the $y-z$ plane (in the E plane) is hemispherical with a theoretical HPBW between 200° and 206° within a frequency range of 11 to 14 GHz (24%), while the radiation in the $x-y$ plane (in the H plane) is a sector beam with an HPBW between 100° and 120°.

From the fact that the radiation pattern is not sensitive to frequency, it is expected that the antenna will have a relatively constant gain over a wide frequency range. The solid line in Fig. 6, showing the theoretical gain G, confirms this expectation. The gain variation is small: the gain G varies between 4.7 dBi and 5.4 dBi within a frequency band of 11 to 14 GHz (24%). The black dots, obtained by using a commercially available electromagnetic wave solver (MW-Studio based on the finite integration method, from CST Corporation), confirm the accuracy of the theoretical gain G.

The theoretical gain G is further confirmed by experimental work. The theoretical gain G [in dBi] (illustrated with a solid line FDTD) and experimental gain (illustrated with white dots) are in good agreement, where both the realized gain G_W and the reflection loss M, defined in Section III, are measured for a 50-ohm feed line and used for the calculation of the experimental gain $G_W[\text{in dBi}] + M[\text{in dB}]$.

Note that the realized gain $G_W[\text{in dBi}](= G[\text{in dBi}] - M[\text{in dB}])$ is smaller than the theoretical gain G in the lower and higher frequency regions, depending on the degree of the reflection loss M due to impedance mismatching between the antenna and the feed line [11], [12].

B. Reduction of the Backward Radiation

So far, we have revealed the antenna characteristics for $(R_{\text{PL}}, B) = (R_{\text{PL50}}, B_{5.6})$. As observed in Fig. 4, the HMA has relatively large backward radiation (radiation in the negative y direction). This section describes one method of reducing the backward radiation. For this, chokes are added to the top and bottom plates of the HMA, as shown in Fig. 7, where each choke has depth d_{ch} and spacing s_{ch}.

We again use parameters $(R_{\text{PL}}, B) = (R_{\text{PL50}}, B_{5.6})$, together with $(d_{\text{ch}}, s_{\text{ch}}) = (0.25\lambda_{12.5}, 0.058\lambda_{12.5})$. Fig. 8 shows the theoretical radiation patterns for two HMAs with and without chokes, as a function of frequency. It is clear that the backward radiation of the HMA with chokes is reduced, compared with that of the HMA without chokes. The backward radiation in the minus y direction is less than -25 dB at a test frequency of 12.5 GHz. The reduction of the backward radiation is attributed to the reduction of the currents flowing on the surfaces of the top and bottom plates.

The reduction in the backward radiation leads to an improvement in the gain. Fig. 9 shows a comparison of the frequency responses between the theoretical gains of the HMAs with and without chokes. The gain of the HMA with chokes is approximately 1 dBi higher than that without chokes. Note that, when a 50-ohm line is used for the HMA with chokes, the realized gain becomes maximal ($G_{W,\max} = 5.9$ dBi) in the vicinity of 12.7 GHz, with a minimum value of 5.1 dBi in the vicinity of 11.6 GHz.

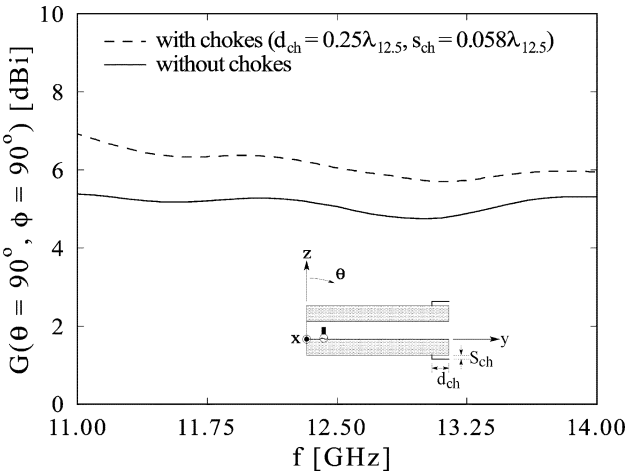

Fig. 9. Gains for half-moon antennas with and without chokes. The radius and thickness of each semi-circular conducting plate are chosen to be $(R_{\rm PL}, B) = (R_{\rm PL50}, B_{5.6}) = (2.08\lambda_{12.5}, 0.233\lambda_{12.5})$.

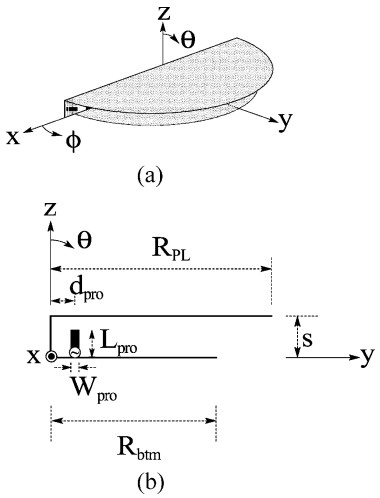

Fig. 10. Modified HMA composed of infinitesimally thin semi-circular conducting plates. (a) Perspective view and (b) side view.

The input impedance $Z_{\rm in}$ of the HMA with chokes as a function of frequency shows almost the same behavior as shown in Fig. 5. It follows that the chokes do not significantly affect the input impedance. The frequency bandwidth for a VSWR $= 2$ criterion is approximately 8.5%.

C. Modified Half-Moon Antenna

This section describes tilted beam formation using an HMA. For this, the radius of the bottom plate $R_{\rm btm}$ is reduced, as shown in Fig. 10. Analysis is performed for an HMA with a top plate of radius $R_{\rm PL} = R_{\rm PL50}$ (fixed) and a bottom plate of radius $R_{\rm btm}$ (variable), assuming that thickness B is infinitesimally thin $(B = 0)$. Other parameters are as defined at the beginning of Section IV.

First, the radiation pattern at 12.5 GHz as a function of the radius of the bottom plate $R_{\rm btm}$ is investigated. Fig. 11 shows representative radiation patterns in the $x - y$ and $y - z$ planes

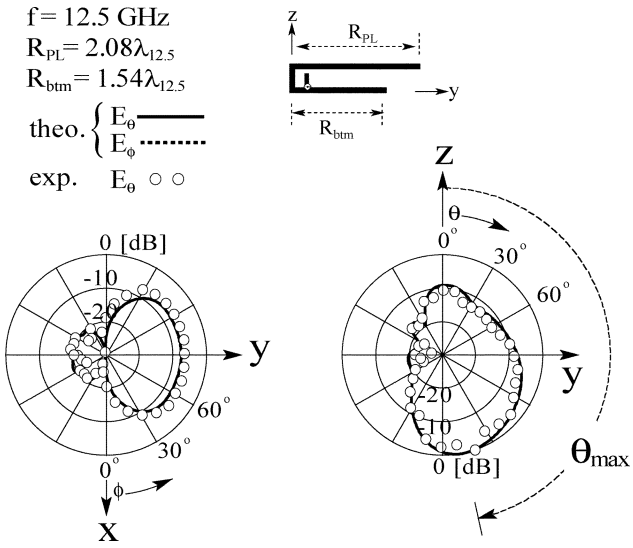

Fig. 11. Representative radiation patterns of a modified HMA.

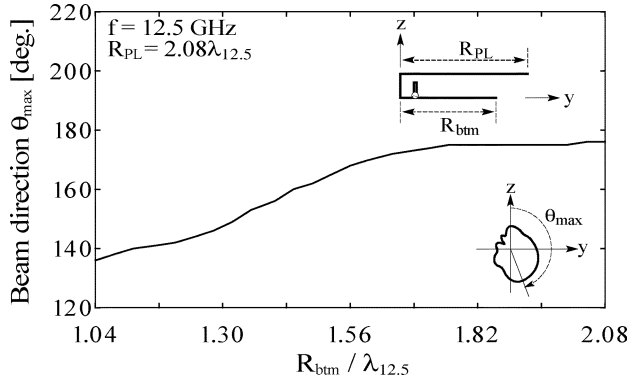

Fig. 12. Maximum beam direction in the $y - z$ plane, $\theta_{\rm max}$, as a function of bottom plate radius $R_{\rm btm}$.

at $R_{\rm btm} = 1.54\lambda_{12.5}$, where the experimental results are presented with white dots. It is found that the radiation is concentrated in the lower hemisphere with a maximum beam direction of $\theta_{\rm max} = 168^\circ$. Note that the theoretical maximum beam direction $\theta_{\rm max}$ in the $y - z$ plane as a function of $R_{\rm btm}$ is shown in Fig. 12. When $R_{\rm btm}$ equals $R_{\rm PL} (= 50\ {\rm mm} = 2.08\lambda_{12.5})$, the radiation pattern in the $y - z$ plane, which has already been shown in Fig. 3(c), has two peaks in the directions $\theta = 176^\circ$ and 4°. In Fig. 12, the value $\theta = 176^\circ$ is used for $\theta_{\rm max}$ at $R_{\rm btm} = 2.08\lambda_{12.5}$.

Next, we focus on a representative modified HMA having a bottom plate radius of $R_{\rm btm} = 1.54\lambda_{12.5}$ and obtain the frequency response. Analysis shows that the maximum beam direction $\theta_{\rm max}$ is not sensitive to frequency. Within a frequency range of 11 to 14 GHz (24%), the maximum beam direction is $\theta_{\rm max} = 167^\circ \pm 2^\circ$.

Fig. 13 shows the theoretical gain G in the maximum beam direction as a function of frequency. The gain G is relatively constant (ranging from 10 dBi to 9 dBi or $G = 9.5 \pm 0.5$ dBi). Note that the realized gain G_W for a 50-ohm feed line shows a maximum value of approximately 9.6 dBi at 12.5 GHz and is reduced to approximately 8.2 dBi at the lower band edge (11 GHz) and 8.3 dBi at the higher band edge (14 GHz).

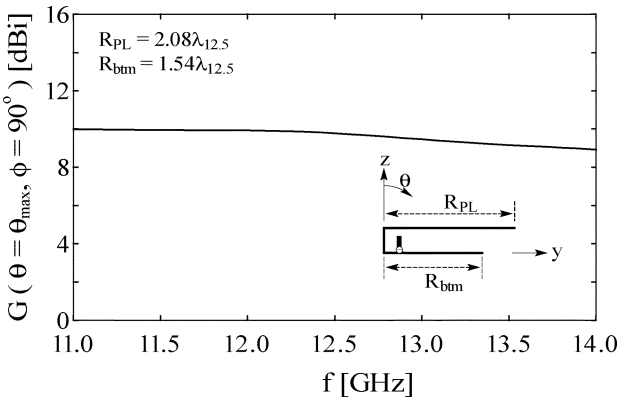

Fig. 13. Gain as a function of frequency.

V. Conclusion

An HMA is proposed to realize a wide radiation beam with a simple structure, which is often required for wireless LAN antennas. The HMA, composed of two semi-circular conducting plates of radius $R_{\rm PL}$, is fed by a probe near a rectangular conducting plate joining these two semi-circular plates. The spacing between the two semi-circular plates is chosen to be less than one-half of the wavelength at a test frequency of 12.5 GHz. The analysis is performed using an FDTD method based on a cylindrical coordinate system.

The analysis shows that an appropriate thickness of the semi-circular plates B, expands the radiation in the y-axis direction (the front of the aperture), increasing to the same value as that in the z-axis direction. Within a frequency band of 11 to 14 GHz (24%), the radiation in the E plane of a representative HMA (the semi-circular plates have a radius of $R_{\rm PL} = 2.08\lambda_{12.5}$ and a thickness of $B = 0.233\lambda_{12.5}$) is hemispherical with an HPBW between 200° and 206°, while the radiation in the H plane is a sector beam with an HPBW between 100° and 120°. Within the same frequency band, the gain varies between 4.7 and 5.4 dBi. Further analysis shows that adding chokes to the semi-circular plates reduces the backward radiation. The representative HMA with chokes has a backward radiation level of less than -25 dB at a test frequency of 12.5 GHz.

Finally, this paper refers to a modified HMA, where the radius of the semi-circular bottom plate is reduced. It is found that the modified HMA radiates into the lower hemisphere, forming a tilted beam. The maximum beam direction of a modified HMA (infinitesimally thin semi-circular top and bottom plates have radii of $R_{\rm PL} = 2.08\lambda_{12.5}$ and $R_{\rm btm} = 1.54\lambda_{12.5}$, respectively) is not sensitive to frequency. Within a frequency range of 11 to 14 GHz (24%), the maximum beam direction in the $y - z$ plane is $\theta_{\max} = 167^{\circ} \pm 2^{\circ}$ and the gain is $G = 9.5 \pm 0.5$ dBi. The modified HMA can be used, for example, as a base station antenna.

Acknowledgment

The authors thank Mr. V. Shkawrytko for his assistance in the preparation of this manuscript.

References

[1] R. C. Johnson, *Antenna Engineering Handbook*, 3rd ed. New York: McGraw Hill, 1993, pp. 40-3–40-4.
[2] A. Taflove, *Computational Electrodynamics*. Norwood, MA: Artech House, 1995.
[3] K. S. Yee, "Numerical solution of initial boundary value problems involving Maxwell's equations in isotropic media," *IEEE Trans. Antennas Propagat.*, vol. AP-14, no. 3, pp. 302–307, May 1966.
[4] N. Dib and T. Weller, "Two-dimensional finite difference time domain analysis of cylindrical transmission lines," *Int. J. Electromagn.*, vol. 87, no. 9, pp. 1065–1081, 2000.
[5] ——, "Finite difference time domain analysis of cylindrical coplanar waveguide circuit," *Int. J. Electromagn.*, vol. 87, no. 9, pp. 1083–1094, 2000.
[6] I. Wako, T. Yagi, and H. Nakano, "Half-moon antenna," in *Proc. Communications Society Conf. IEICE*, Funabashi, Japan, Sept. 1999, p. B-1-45.
[7] Y. Yamamoto, M. Sugama, J. Yamauchi, and H. Nakano, "Numerical analysis of a half-moon antenna," in *Proc. Communications Society Conf. IECE*, Funabashi, Japan, Sept. 1999, p. B-1-46.
[8] H. Nakano, Y. Yamamoto, M. Ikeda, and J. Yamauchi, "A half-moon antenna," in *Proc. IEEE AP-S Int. Symp.*, San Antonio, June 2002, pp. 840–843.
[9] Z. P. Liao, H. L. Wong, B. P. Yang, and Y. F. Yuan, "A transmitting boundary for transient wave analysis," *Science Sinica*, ser. A, vol. 27, no. 10, pp. 1063–1076, 1984.
[10] R. F. Harrington, *Time-Harmonic Electromagnetic Fields*. New York: McGraw-Hill, 1961, pp. 106–110.
[11] Y. Mushiake, *Antenna and Propagation* Corona, Tokyo, 1973, p. 113.
[12] Y. T. Lo and S. W. Lee, *Antenna Handbook*. New York: Van Nostrand Reinhold, 1988, ch. 1, pp. 1.24–1.25.
[13] H. Nakano, J. Eto, Y. Okabe, and J. Yamauchi, "Tilted- and axial-beam formation by a single-arm rectangular spiral antenna with compact dielectric substrate and conducting plane," *IEEE Trans. Antennas Propagat.*, vol. 50, no. 1, pp. 17–24, Jan. 2002.
[14] C. A. Balanis, *Antenna Theory*. New York: Harper and Row, 1982, p. 338.
[15] K. Kunz and R. J. Luebbers, *The Finite Difference Time Domain Method for Electromagnetics*, Boca Raton, FL: CRC Press, 1993, pp. 370–389.

Hisamatsu Nakano (M'75–SM'87–F'92) received the B.E., M.E., and Dr.E. degrees in electrical engineering from Hosei University, Tokyo, in 1968, 1970, and 1974, respectively.

Since 1973, he has been a Member of the Faculty of Hosei University, where he is now a Professor in the Electronic Informatics Department. From March to September 1981, he was a Visiting Associate Professor at Syracuse University; from March to September 1986 a Visiting Professor at the University of Manitoba; and from September 1986 to March 1987 a Visiting Professor at the University of California, Los Angeles. In 2001, he was appointed to the Guest Professorship of Shanghai Jiao Tong University, China. One of his most significant contributions is the development of a parabolic reflector antenna using a backfire helical feed for reception of direct broadcast satellite (DBS) TV programs. He has also contributed to the development of two types of small flat DBS antennas using curled and helical elements. He has published more than 190 refereed journal papers, more than 160 international symposium papers, and more than 500 national symposium papers. He is the author of *Helical and Spiral Antennas* (Hertfordshire, U.K., New York: Research Studies Press, Wiley, 1987) and coauthor of *Analysis Methods of Electromagnetic Wave Problems* (Norwood, MA: Artech House, vol. 2, 1996). His research topics include numerical methods for low- and high-frequency antennas and optical waveguides.

Dr. Nakano received the IEE International Conference on Antennas and Propagation Best Paper Award and the IEEE Transactions on Antennas and Propagation Best Application Paper Award (H. A. Wheeler Award), in 1989 and 1994, respectively. In 1992, he was elected an IEEE fellow for contributions to the design of spiral and helical antennas. In 2001, he received the Award of Distinguished Technical Communication (from the Society for Technical Communication, USA). He is an Associate Editor of several journals and magazines, such as *Electromagnetics*, IEEE Antennas and Propagation Magazine, IEEE Antennas and Wireless Propagation Letters, and *Asian Information-Science-Life*.

Yusuke Yamamoto was born in Shizuoka, Japan, on May 5, 1976. He received the B.E. and M.E. degrees in electrical engineering from Hosei University, Tokyo, Japan, in 2000 and 2002, respectively.

He joined Canon Incorporated, Tokyo, in 2002.

Mr. Yamamoto is a Member of the Institute of Electronics, Information and Communication Engineers (IEICE) of Japan.

Masaaki Seto was born in Kanagawa, Japan, on October 3, 1979. He received the B.E. and M.E. degrees in electrical engineering from Hosei University, Tokyo, Japan, in 2002 and 2004, respectively.

He joined NEC Corporation, Tokyo, in 2004.

Mr. Seto is a Member of the Institute of Electronics, Information and Communication Engineers (IEICE) of Japan.

Kazuo Hitosugi was born in Kanagawa, Japan, on July 30, 1979. He received the B.E. degree in electrical engineering from Hosei University, Tokyo, in 2003, where he is currently working toward the M.E. degree.

Mr. Hitosugi is a Member of the Institute of Electronics, Information and Communication Engineers (IEICE) of Japan.

Junji Yamauchi (M'85) was born in Nagoya, Japan, on August 23, 1953. He received the B.E., M.E., and Dr.E. degrees from Hosei University, Tokyo, Japan, in 1976, 1978, and 1982, respectively.

From 1984 to 1988, he served as a Lecturer in the Electrical Engineering Department, Tokyo Metropolitan Technical College. Since 1988, he has been a Member of the Faculty of Hosei University, where he is now a Professor in the Electronic Informatics Department. He is the author of *Propagating beam analysis of optical waveguides* (Hertfordshire, U.K.: Research Studies Press, 2003). His research interests include optical waveguides and circularly polarized antennas.

Dr. Yamauchi is a Member of the Optical Society of America (OSA) and the Institute of Electronics, Information and Communication Engineers (IEICE) of Japan.